Hindawi
Mathematical Problems in Engineering
Volume 2021, Article ID 6255014, 10 pages
https://doi.org/10.1155/2021/6255014

*Research Article*

# Study on Impact Resistance of C/SiC Ceramic Matrix Composites for Thermal Protection of the Aerospace Vehicle

**Ye Lin**[1] **and Bin Liu**[2]

[1]*Beijing Aerospace Technology Institute, Beijing, China*
[2]*School of Aeronautics, Northwestern Polytechnical University, Xi'an, China*

Correspondence should be addressed to Ye Lin; linye1615@sina.com

Received 23 June 2021; Accepted 14 August 2021; Published 23 August 2021

Academic Editor: Chengwei Fei



This paper evaluates the impact damage tolerance of ceramic matrix composites and contrasts their tensile and compression strengths under impact and nonimpact conditions. The representative C/SiC composites from PIP are examined under the dropped tip system. In this paper, the surface impact test of C/SiC composites is carried out. By testing a series of specimens of various impact energies, the tensile and compression properties after impact are studied. Meanwhile, by comparing the changes of the specimens after impact and nonimpact, the fracture process, fracture modes, and residual strength are investigated. The results indicate that the residual tensile strength after impact reduces greatly, compared with the nonimpact material, by about 25%–45%, while the compression strength reduces slightly. The residual strength of tension and compression illustrates that low-energy impact effect on the structural integrity must be given priority in the thermal protection structure design of astronautics and aeronautics.

## 1. Introduction

Ceramic matrix composites have been successfully used in high-temperature components in aerospace due to their excellent strength of high temperature, low density, good oxidation resistance, and wear resistance. For example, by applying in scramjets, C/SiC composite material can simplify the structure, reduce the weight, and significantly improve the comprehensive performance of the engine and the payload of the aircraft. Meanwhile, it has become one of the pivotal high-temperature-resistant materials for the thermal protection structure of the hypersonic aircraft in nearby space [1, 2]. With the urgent demand of high thrust-to-weight ratio and high working temperature for aeroengines, ceramic matrix composites are gradually used as hot-end components of aeroengines, such as blades.

As for the external structure of space vehicles, their service performance will inevitably be impacted by foreign objects during their services and maintenance. C/SiC composite material has a good static performance. However, poor performance caused by foreign object damage (FOD) may limit its applicability as a primary bearing structure [3, 4]. For instance, the Space Shuttle 'Columbia' was cracked after being hit on the SiC-C/C plate [5]. The fracture damage and disintegration caused by cracks are related to the defect and mechanical damage of the ceramic matrix composite. Therefore, it is particularly important and challenging to study the impact damage and impact resistance about ceramic matrix composites [6–8]. For the components in the hot end of aeroengines, the most likely impact sources during their services are medium-high speed and low-energy impact. These may result in internal damage to the material and a decrease in structural strength. Recent literature has focused on the impact damage and postimpact bearing capacity of sand, metal, and other particles. In 2010, Ogi et al. [9] studied on the impact damage of 2D- and 3D-woven CMC plates with the condition of impact energy from 0.7 J to 20 J (whose impact velocities were between 200 m/s and 1200 m/s). By being impacted at different velocities, the surface and the internal damage were observed and compared. In 2019, Presby et al. [10] investigated the impact by the 1.59 mm steel ball on the SiC/SiC composite plate and

bent plates at 340 m/s (with an impact energy of 6.5 J) by combining experimental and numerical methods.

At present, the discussion on the impact damage of external objects upon ceramic matrix composites at a low speed is mostly based on the external thermal protection structure of the spacecraft, such as tool drop during repair, collision during transportation, and even the impact of gravel and hail from runway during takeoff and landing. In 2006, Trabandt et al. [11] studied on the weather environment adaptability research program, which focused on the reusable thermal protection system on the ground and track. C/SiC composites were used for the 0.7–12 J low-velocity impact experiment. It revealed that, in the condition of the impact energy of less than 0.7 J, the material damage was not serious. The environmental performance of materials was affected inconspicuously, and it was unnecessary to change the parts. Nevertheless, if the impact energy is more than 1 J, there will be serious internal delamination in the material. Therefore, when the ceramic matrix composites are impacted by low energy, the internal damage will occur definitely, which may be invisible on the surface of the material with the naked eyes and needs characterizing [12, 13]. In 2012, impact damage at a low speed, response, and residual tensile strength of 3D-woven SiC/SiC composites were studied by Herb et al. [14]. Then, in 2016, Mei et al. [15] conducted an experimental study on low-speed impact and tensile bearing capacity of 2D C/SiC composites by testing a series of different seam densities. In 2017, Mei et al. [16] observed the impact impedance and residual tensile strength of C/SiC composites in the condition of different levels of impact energy. In 2016, based on the simulation about the improved Hashin–Rotem criterion and cohesion model, a progressive damage model was established by Li and Hoo Fatt [17]. Meanwhile, the impact was numerically simulated for 2D-woven SiC/SiC composites. In 2015, Yang et al. [18] conducted the impact experiment with midspeed of the 2D C/SiC plate based on the air gun device in the range of 79–219 m/s. The numerical simulation results were carried out to deduce the formula for predicting the ultimate penetration depth of C/SiC material impacted by the steel projectile. It thus appears that there have been a gradually increasing number of research studies on the performance and damage of ceramic matrix composites at low speed and of low energy in recent years. However, the description of the impact response and impact damage was not deep enough, with less adequate investigations on their impact resistance and residual strength.

From what we have discussed above, it can be found that the foreign object impact on the ceramic matrix composite structure for thermal protection of the spacecraft is at low speed and of low energy, while the impact of small particles on the turbine blade of the ceramic matrix composite material of the aircraft engine is at medium and high speeds and of low energy. This paper focuses on the impact of the low-speed and low-energy impact service environment on C/SiC composite materials and proposes an experimental study on the mechanical performance of C/SiC ceramic matrix composites under axial tensile and compressive impact loading.

## 2. Experimental Methods

*2.1. Specimen Preparation.* C/SiC ceramic matrix composite was tested in this paper. PIP was successfully adopted to prepare the experiment specimens. Precursor infiltration pyrolysis (PIP) is an effective method to synthesize ceramics in the porous preform due to the ceramic distribution uniformity and the ceramic component designability [19]. In PIP, carbon fibrous preform is infiltrated into the precursor-mixed solution under the vacuum pressure condition. Then, after curing, cross-linking, and pyrolysis, it is transformed into the inorganic ceramic matrix. This is particularly advantageous for the preparation of the jumbo-sized and complex components because of its low pyrolysis temperature, changeable components, and uniformly dispersed ceramic matrix.

The micromorphology of the specimen was observed by the technique of micro-CT scanning. The micrograph of the external surface and internal surface of the material is shown in Figures 1(a) and 1(b).

In order to ensure the impact effect, the overall width of the tension specimen was made large so that it could bear larger tension load. Specimens were designed and wedged in such a way that they were able to be held steadily and easy to be loaded. The tension specimen diagram is shown in Figure 2(a), where $H1 = 60$ mm, $H2 = 74.25$ mm, $L1 = 60$ mm, $L2 = 150$ mm, and the thickness is 6 mm. The specimen for the compression test is a rectangular composite plate as shown in Figure 2(b) (150 mm long and 100 mm wide).

*2.2. Experimental Methods and Setup.* In this paper, first of all, energy screening tests (impact testing at various energies) were carried out for 10 C/SiC composite plates in each group, respectively, and the damage areas were observed after impacts. Then, the tension properties and compression properties of the 2 groups of C/SiC composites, containing impact damage and nonimpact damage, were tested at room temperature after impact. In the tension experiments, the specimens were divided into three groups, including 5 nonimpact specimens, 15 postimpact specimens of 10 J, and 5 postimpact specimens of 12 J. There were two groups of specimens for compression experiments as well, including 4 nonimpact damage ones and 12 postimpact ones of 10 J.

The impact test refers to the ASTM D7136/D7136M-12 standard [20] which uses double-column drop hammer impact equipment, as shown in Figure 3. The maximum height of the drop hammer is 1.5 m and the maximum mass is 11.5 kg which meet the test requirements. The clamping way for the compression specimens is shown in Figure 4(a) and for tension specimens is shown in Figure 4(b).

The Instron 1000 HDX static hydraulic universal material testing machine was employed to test the tension properties, with the maximum load of 1000 kN. Meanwhile, the compression after impact (CAI) setup and sample installation for compression experiments are shown in Figure 5. CAI is a method to evaluate the damage tolerance of composite material systems and structures. According to the specified pit depth, CAI can be used to determine the limit value for design, which is the residual compressive strength or failure strain containing the specified damage.

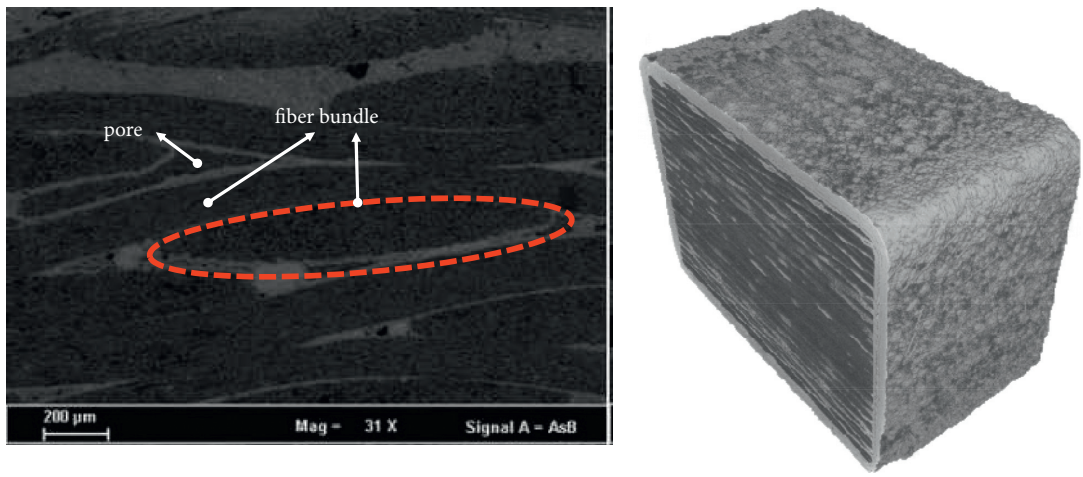


(a) (b)

Figure 1: (a) The micrograph of the external surface. (b) The micrograph of the internal surface of the material.

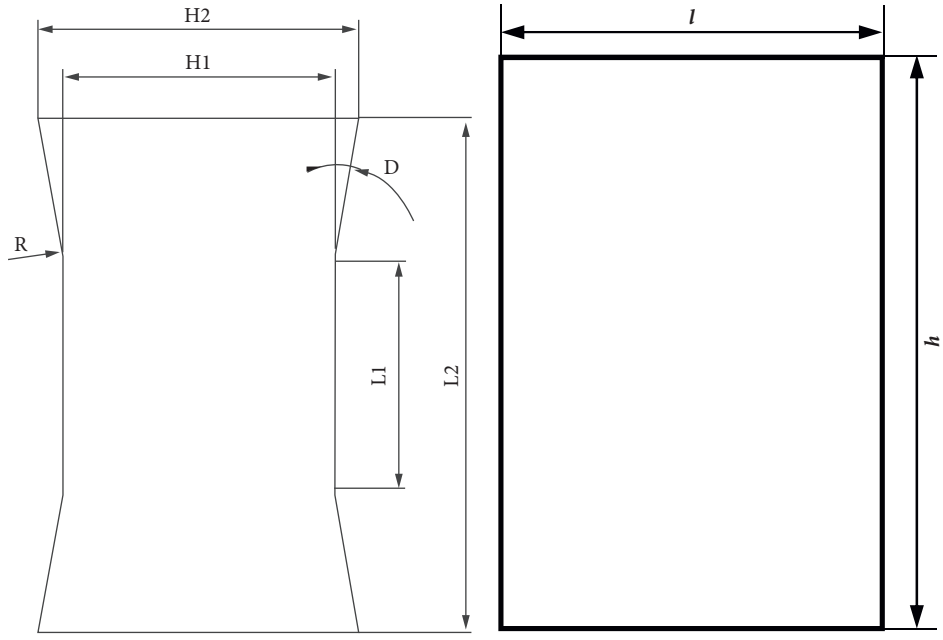


(a) (b)

Figure 2: The tension specimen diagram (a) and the compression specimen diagram (b).

## 3. Experimental Results and Analysis

*3.1. Impact Load and Impact Damage.* Accompanied with the destruction of the fiber and matrix, the crack on the back of the specimen exhibited an "X" pattern (Figure 6(a)). With the increase of impact energy, the impact damage volume from both front and back of the specimen was increasingly serious. The impact damage dimension matrix for the two groups can be described in Tables 1 and 2. Meanwhile, corresponding to 10 J and 12 J, respectively, 1-3# and 1-4# have been found to be able to realize the test effect of damage which was visually obvious between some limited changes of impact energy.

The impact damage volume of the specimen can be illustrated from two aspects. From the in-plane damage, the damage on the back varies as an elliptic shape (Figure 7), while the long axis $2a$ and the short axis $2b$ of the ellipse grow with the increase of impact energy. On the contrary, the depth of the pit also increases nonlinearly with the increase of impact energy. In the second group of experiments, some pit depths reduced while the energy increased, which may be related to the significant increase in the diameter of pits. Figure 8 shows the statistics of pit depths in the case of different energies. It can be seen that, with the increase of impact energy, the pit depth presents an overall rising trend, and the increasing trend is faster and faster.

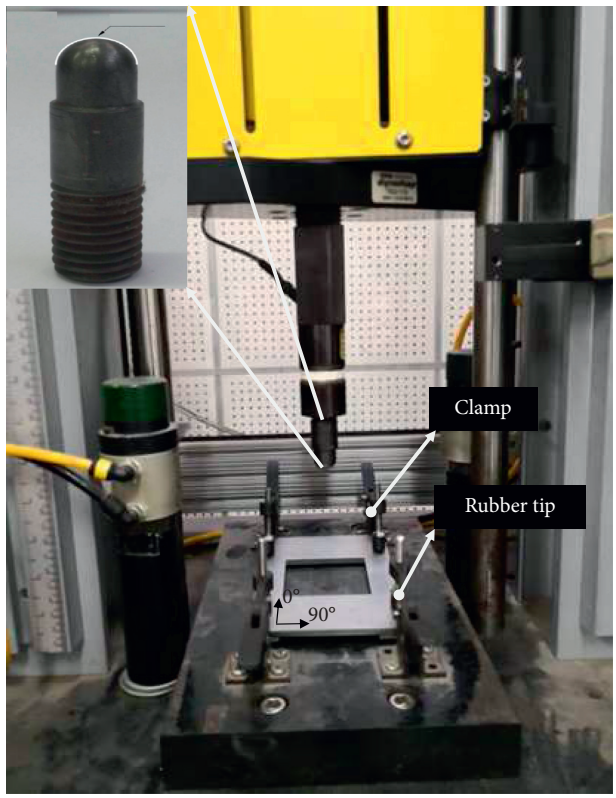


Figure 3: Dropped tip fixture by redesigning [21, 22].

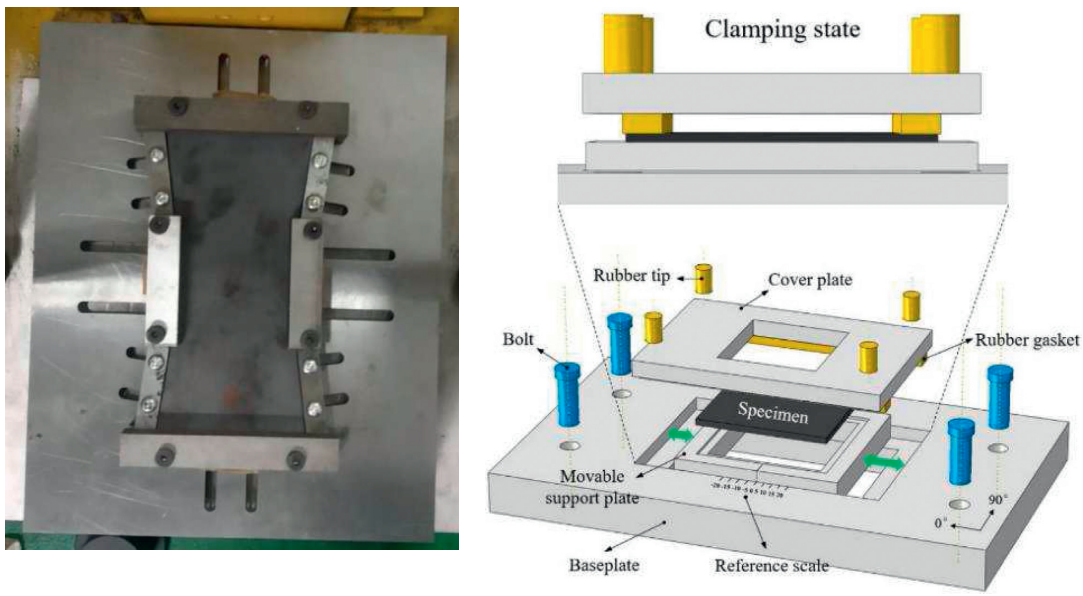


(a) (b)

Figure 4: The clamping way for impact. (a) Tension specimen. (b) Compression specimen.

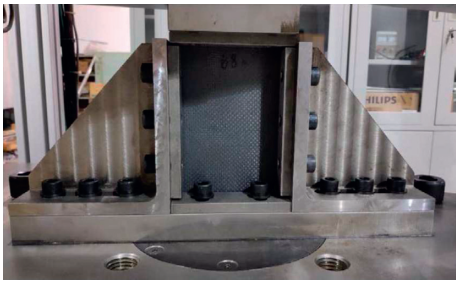

Figure 5: CAI setup and sample installation.

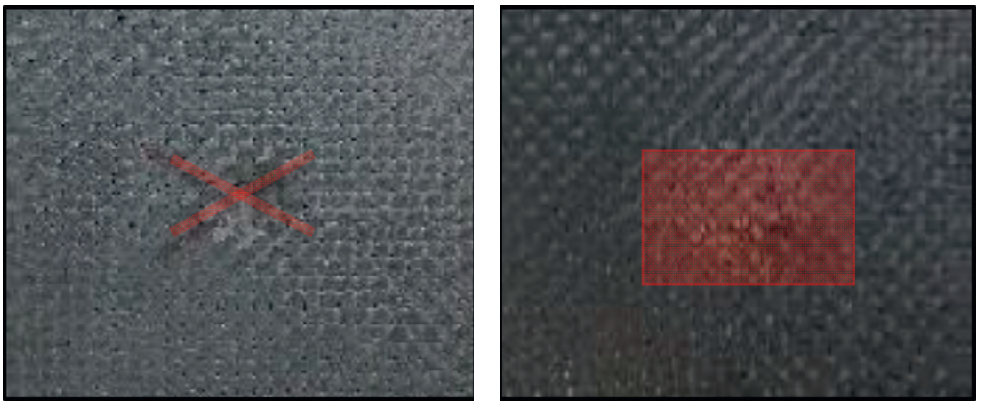

(a) (b)

Figure 6: Damage from the front side and back side of 1-4#.

Table 1: Impact damage of group 1.

| No. | Impact energy (J) | Front-damage diameter (mm) | Front-damage depth (mm) | Back-damage dimension (mm) |
|---|---|---|---|---|
| 1-1# | 6 | 4.81 | 0.447 | $14.59 \times 9.63$ |
| 1-2# | 8 | 6.61 | 0.591 | $14.77 \times 9.05$ |
| 1-3# | 10 | 9.61 | 1.156 | $17.69 \times 15.57$ |
| 1-4# | 12 | 11.47 | 1.218 | $18.02 \times 14.47$ |
| 1-5# | 14 | 11.53 | 2.039 | $21.37 \times 17.28$ |
| 1-6# | 16 | 12.23 | 2.106 | $21.14 \times 17.83$ |
| 1-7# | 18 | 13.00 | 3.607 | $19.78 \times 18.84$ |
| 1-8# | 20 | 13.05 | 4.354 | $21.69 \times 20.47$ |
| 1-9# | 10 | 8.20 | 0.995 | $17.32 \times 16.38$ |
| 1-10# | 12 | 12.20 | 2.852 | $17.81 \times 17.77$ |

Table 2: Impact damage of group 2.

| No. | Impact energy (J) | Damage diameter (mm) | Damage depth (mm) |
|---|---|---|---|
| 2-1# | 7 | 5.43 | 0.317 |
| 2-2# | 8 | 6.66 | 0.320 |
| 2-3# | 9 | 7.40 | 0.465 |
| 2-4# | 10 | 8.11 | 0.685 |
| 2-5# | 11 | 8.62 | 0.678 |
| 2-6# | 12 | 9.35 | 0.566 |
| 2-7# | 13 | 10.21 | 0.633 |
| 2-8# | 14 | 11.13 | 0.852 |
| 2-9# | 9 | 7.36 | 0.515 |
| 2-10# | 11 | 8.65 | 0.731 |

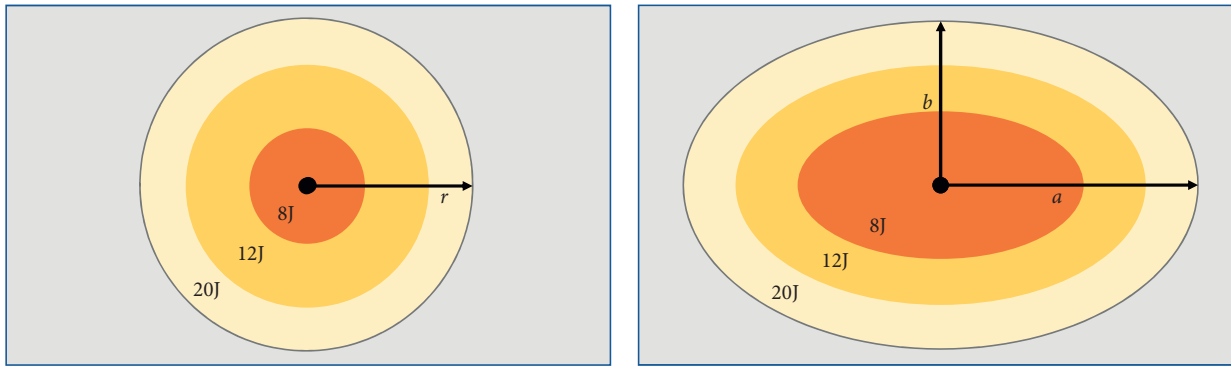


(a) (b)

Figure 7: In-plane damage under different energies. (a) Damage diagram of the front side. (b) Damage diagram of the back.

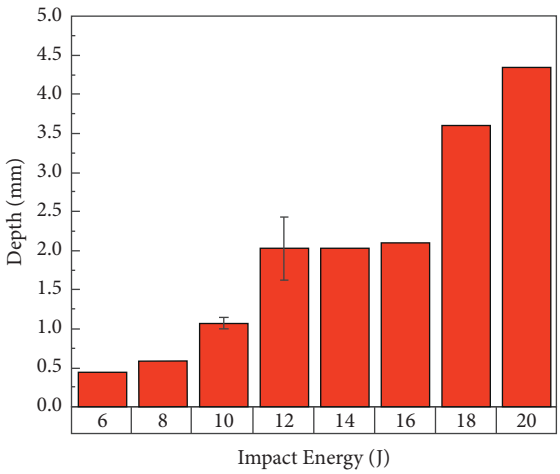


Figure 8: Pit depth under different energies.

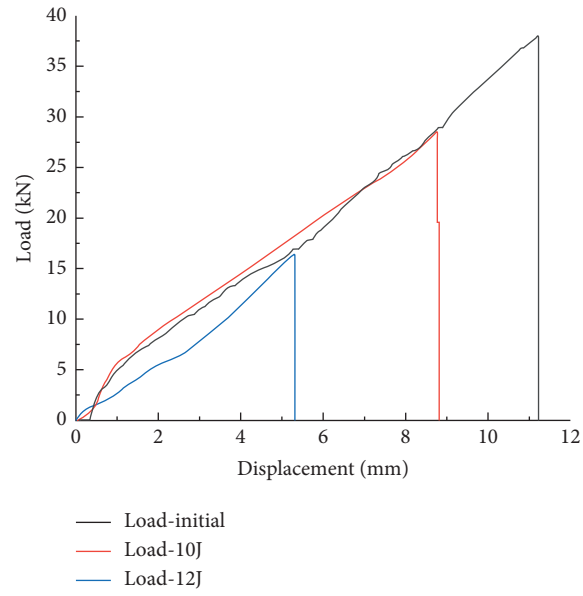


Figure 9: Tension load-displacement curve (typical curves).

### 3.2. Influence of Impact Energy on Residual Tensile Strength

*3.2.1. Load-Displacement Curve Analysis.* Contrasting the load-displacement curve of the tension test (Figure 9) between nondestructive materials and materials containing impact damage, it can be proved that the tension load on the damaged materials is much lower than that on the nondestructive ones, i.e., the tensile load of the specimens after the impact load of 10 J reduced to 27 kN, while that after the impact load of 12 J decreased to about 16 kN, which is only 42.7% of the undamaged condition.

*3.2.2. Macrodamage Morphology Analysis.* By observing the specimens after tension tests, it can be found that the failure positions of the specimens without impact are mostly at the connection of transition sections and parallel sections. There is no obvious stratification at the fracture but rattled at the break. As is illustrated in Figure 10, all specimens subjected to 10 J impact were destroyed at the impact position. In addition, the fracture position shows obvious fiber fracture, which was not smooth, and some even show obvious stratification. During loading, the sound frequency gradually increased until it was completely destroyed. After 12 J impact, all the specimens were damaged in the middle (i.e., the impacted position). However, the fracture is relatively smooth, with a small amount of fiber pulling out and no stratification compared with the 10 J specimen.

*3.2.3. Calculation of Residual Strength.* The failure load is calculated by the load-displacement curve of the specimen. In the case of the conventional nondestructive state, the tensile strength of the C/SiC composite specimen is calculated by

$$\sigma = \frac{P_{\max}}{A}. \tag{1}$$

However, for the specimen after impact, its cross section is not a rectangle but contains irregular-shaped impact pits. Regarded as a semiellipse in the calculation process, its short half axis is pit depth, and the long half axis is pit radius. Hence, the cross-sectional area of the specimen is $A = S_{\text{rectangular}} - S_{\text{semiellipse}}$.

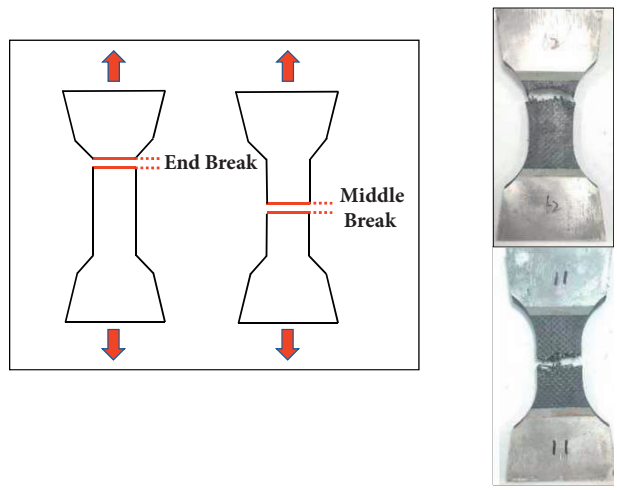


Figure 10: The fracture morphology in tension tests: nonimpacted material (a) and damaged material by 10 J/12 J impact (b).

Table 3: Maximum tensile load and tensile strength.

| | Impact energy | The average maximum tensile load | The average tensile strength | The percentage of residual strength |
|---|---|---|---|---|
| Nondestructive | 0 | 37.60 | 273.78 | 100 |
| Impact | 10 | 24.18 | 186.57 | 68.17 |
| | 12 | 18.45 | 140.90 | 51.46 |

The tensile strength and residual strength percentage of each specimen were calculated (Table 3). The residual tensile strength of three groups is shown in Figure 11.

Therefore, with the increase of impact energy, the maximum tensile load and tensile strength decrease obviously. The residual strength of the specimen with an impact energy of 10 J decreased to about 70% of the nondestructive specimen. Meanwhile, the residual strength of the specimen with an impact energy of 12 J decreased to about 55% of the nondestructive specimen. The results indicated that impact function is the main reason for the reduction of tensile strength.

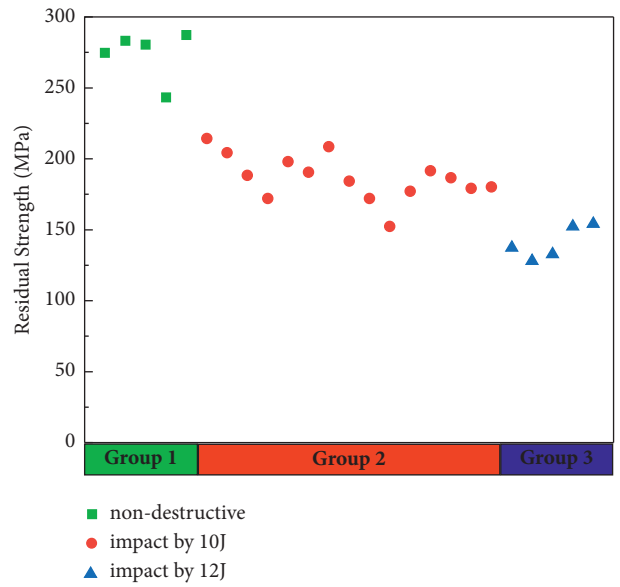


Figure 11: Residual tensile strength of three groups.

### 3.3. Influence of Impact Energy on Residual Compression Strength

*3.3.1. Load-Displacement Curve Analysis.* Comparing the load-displacement curves between the compression experiments of nondestructive materials and materials containing damage (Figure 12) indicates that there are fluctuations in the maximum load. It should be noted that the maximum compression load of some specimens even exceeds the maximum load of compression in the nondestructive state.

*3.3.2. Macrodamage Morphology Analysis.* The compression test specimen consisted of two groups, 4 specimens without impact and 12 specimens after 10 J impact. As shown in Figure 13, the failure mode of the specimen without impact was dominated by a collapse at the boundary of the loading end. In contrast, transverse failure occurred in the middle part of the specimen with the damage of 10 J impact energy. The specimens showed various levels of bending, and the failure direction gradually expanded to the two sides perpendicular to the loading direction on the basis of the initial damage position. For the final damage morphology, the failure that appeared in the direction of 45° or −45° in the middle could be found, and the failure in the horizontal direction on both sides of the middle parts (Figure 13) was shown as well.

By observing the damaged area, as is shown in Figure 14, it can be seen that different degrees of bulges and fiber damage fracture appear on the front, and fiber fracture stratification appears on the side.

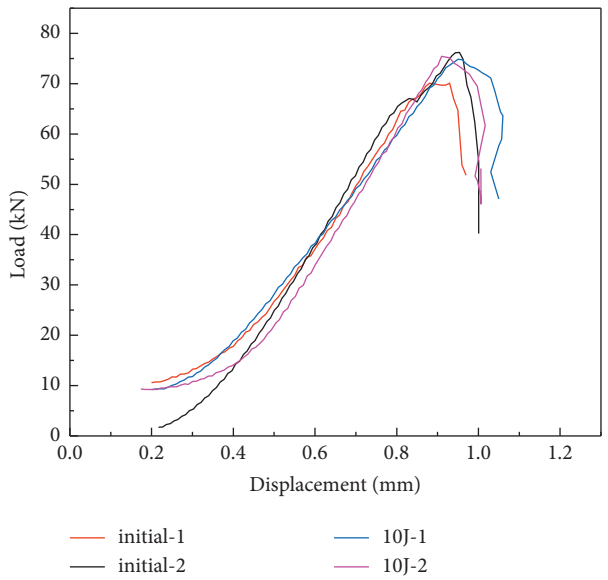


Figure 12: Compression load-displacement curve (typical curves).

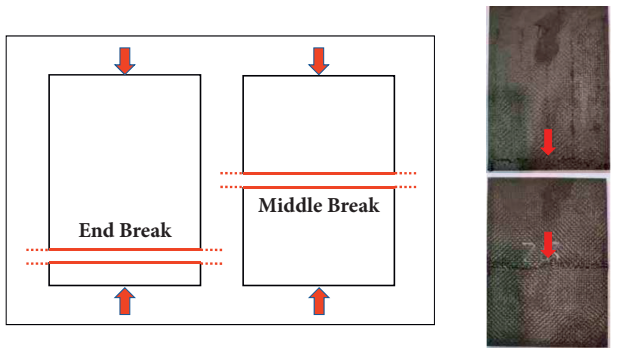


Figure 13: The fracture morphology in compression tests: non-impacted material (a) and damaged material by 10 J impact (b).

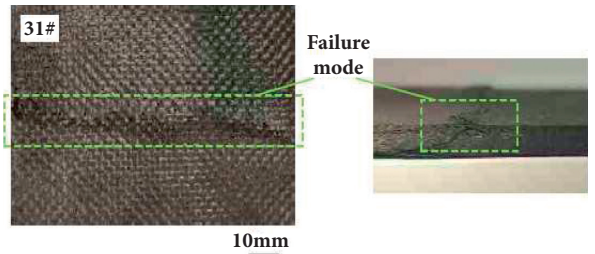


Figure 14: Compression damage diagram of the damaged specimen with 10 J impact load.

Four strain gauges were affixed on both sides of the pit and both faces of the specimen (Figure 15). The peak impact force was collected at 3887.3 N and 4152.8 N, respectively. The stress-time curve is shown in Figure 16. At the beginning of compression, the strain value of $S_1$–$S_4$ changed synchronously with little change, which indicated that the whole

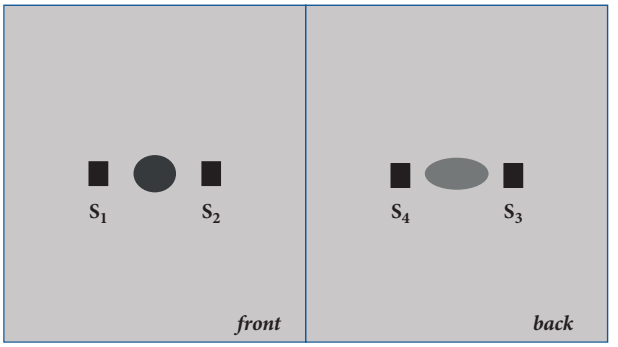


Figure 15: Schematic diagram of the strain gauge.

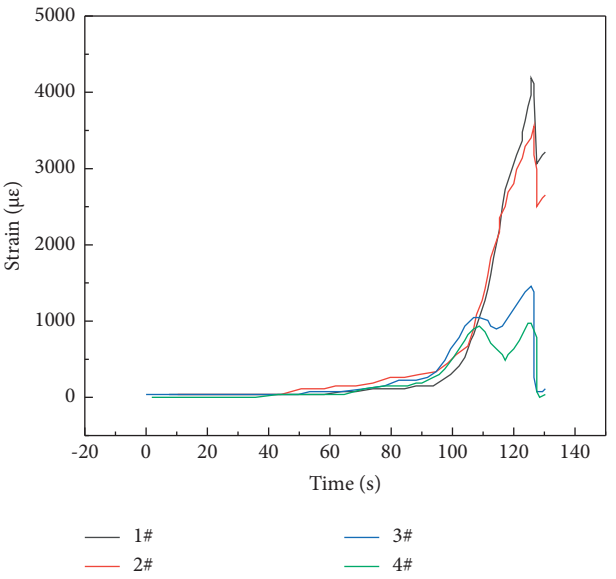


Figure 16: Strain-time curve.

specimen was in the compression state without bending or failure. However, with the increase of the compression displacement and the continuous failure of the specimen, the strain-time curve began to show a large upward trend, and finally, the failure occurred under the ultimate failure load. It can be seen that the final strain values of $S_1$ and $S_2$ are significantly different from those of $S_3$ and $S_4$, showing that the specimen was bent at this time which caused the difference of strain values on the front and back of the specimen.

*3.3.3. Calculation of Residual Strength.* Table 4 shows the calculation of the residual strength of the compression test. Compared with the nondestructive materials, the maximum compressive load and compressive strength of the specimen with an impact energy of 10 J do not exhibit significant change after compression. Besides, the residual strength declines by no more than 15%. In addition, the residual strength of some damaged specimens even exceeds the strength under the nondestructive state (Figure 17).

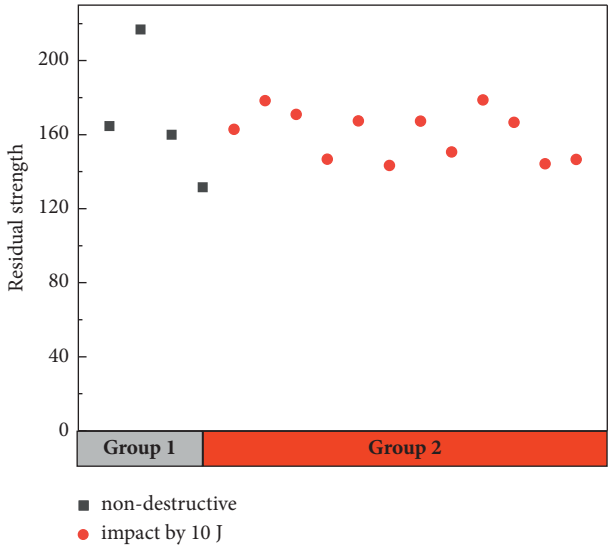


Figure 17: Residual tensile strength of three groups.

Table 4: Maximum compression load and compression strength.

| | Impact energy | The average maximum compressive load | The average compressive strength | The percentage of residual strength |
|---|---|---|---|---|
| Nondestructive | 0 | 77.48 | 168.30 | 100 |
| Impact | 10 | 72.03 | 160.28 | 95.23 |

## 4. Conclusion

In this paper, a series of impact energy screening tests were carried out on C/SiC ceramic matrix composites. And the impact velocity and impact force were successfully measured. At the same time, tension and compression properties after impact were studied. Meanwhile, the fracture process and residual strength were analyzed. According to the experimental studies, the following conclusions can be drawn:

(1) Impact tests of C/SiC composite materials in the condition of two groups of 16 different impact energies were carried out. The results show that, with the increase of impact capacity, the damage area and pit depth in the damaged area of the specimen also increase. And the destruction mode exhibits as the destruction of the matrix and fiber. Under the impact energy from 10 J to 12 J, it presents a significant damage effect visually with a small change in energy.

(2) The tension and compression properties of the materials after impact and the compression properties of the specimens after impact were studied, respectively. During the tension tests, the fracture surfaces of the specimens were all located in the center of the pit, while those of the nondestructive specimens were mostly at the connection of the transition sections and parallel sections. Besides, during the compression test, the middle of the damaged specimens appears bending, while the nonimpacted specimens appear crushing at the loading end.

(3) The analysis of the residual strength of the postimpact tensile and postimpact compression specimens reveals that, after impact, the tensile strength of C/SiC composite material was greatly reduced, compared with the nonimpact state, by about 25%–45%, while the compression strength was slightly reduced.

From this study, the residual strength under tensile load after impact is greatly reduced. In the future, appropriate ways can be adopted to improve the residual strength as far as possible, such as by designing layering and changing the thickness of the single layer and the whole thickness.

## Data Availability

Sequence files and metadata for all samples that support the findings of this study are openly available at https://doi.org/10.6084/m9.figshare.14806182.v1.

## Conflicts of Interest

The authors declare that they have no conflicts of interest.

## Acknowledgments

The authors would like to thank the National Natural Science Foundation of China (contract no. 51902256), Aeronautical Science Foundation of China (contract no. 2020Z057053002), and Chinese National Foundation for Natural Sciences (contract no. 5000200389) for the support in this research.

## References


[1] M. Qingsong, L. Hatao, P. Yu et al., "Research progress on the application of C/SiC composites in scramjet," *Journal of Inorganic Materials*, vol. 28, no. 3, pp. 247–255, 2013, in Chinese.

[2] L. Han, Y. B. Wang, Y. Zhang, C. Lu, C. W. Fei, and Y. J. Zhao, "Competitive cracking behavior and microscopic mechanism of Ni-based superalloy blade respecting accelerated CCF failure," *International Journal of Fatigue*, vol. 150, Article ID 106306, 2021.

[3] L. Liping, W. Guilin, W. Yiguang et al., "Catalytic performance of C/SiC composites in high enthalpy chemical nonequilibrium flow," *Acta Aeronautica et Astronautica Sinica*, vol. 39, no. 5, pp. 231–239, 2008, in Chinese.

[4] C. Fei, H. Liu, R. Patricia Liem, Y. Choy, L. Han, and L. Han, "Hierarchical model updating strategy of complex assembled structures with uncorrelated dynamic modes," *Chinese Journal of Aeronautics*, 2021, in press.

[5] Z. Aslan, R. Karakuzu, B. Okutan et al., "The response of laminated composite plates under low-velocity impact loading," *Composite Structures*, vol. 59, no. 1, pp. 119–127, 2003.

[6] Z. Litong, C. Laifei, and X. Yongdong, "Progress in research work of new CMC-SiC," *Aeronautical Manufacturing Technology*, vol. 1, pp. 24–32, 2003, in Chinese.

[7] Z. Shiqin, Z. Chagrui, Z. Xingui et al., "Application of continuous fiber reinforced ceramic matrix composites in aeroengine," *Aeroengine*, vol. 31, no. 3, pp. 55–58, 2005, in Chinese.

[8] C. Lu, C. W. Fei, Y. W. Feng, Y. J. Zhao, and X. W. Dong, "Probabilistic analyses of structural dynamic response with modified Kriging-based moving extremum framework," *Engineering Failure Analysis*, vol. 125, Article ID 105398, 2021.

[9] K. Ogi, T. Okabe, and M. Takahashi, "Experimental characterization of high-speed impact damage behavior in a three-dimensionally woven SiC/SiC composite," *Composites Part A: Applied Science and Manufacturing*, vol. 41, no. 4, pp. 489–498, 2010, ISSN 1359-835X.

[10] M. J. Presby, R. Mansour, K. Manigandan et al., "Characterization and simulation of foreign object damage in curved and flat SiC/SiC ceramic matrix composites," *Ceramics International*, vol. 45, no. 2, pp. 2635–2643, 2019.

[11] U. Trabandt, W. Fischer, A. Guelhan et al., "Improvement of lifetime performance of removable TPS and hot structures," in *Proceedings of the 9th AIAA/ASME Joint Thermophysics and Heat Transfer Conference*, pp. 1–10, San Francisco, California, June 2006.

[12] H. R. Xu, L. F. Cheng, and H. Mei, "The characterization of indentation of 2D C/SiC composites subjected to quasi-static indentation," *Acta aeronautica sinica*, vol. 33, no. 8, pp. 1547–1553, 2012, in Chinese.

[13] H. Mei, L. Zhang, H. Xu, and L. Cheng, "Damage mechanism of a carbon fiber ceramic composite during the step-loading indentation and its effect on the mechanical properties," *Composites Part B: Engineering*, vol. 56, pp. 142–148, 2014.

[14] V. Herb, E. Martin, and G. Couégnat, "Damage analysis of thin 3D-woven SiC/SiC composite under low velocity impact loading," *Composites Part A: Applied Science and Manufacturing*, vol. 43, no. 2, pp. 247–253, 2012.

[15] H. Mei, C. Yu, H. Xu, and L. Cheng, "The effects of stitched density on low-velocity impact damage of cross-woven carbon fiber reinforced silicon carbide composites," *Ceramics International*, vol. 42, no. 1, pp. 1762–1768, 2016.

[16] H. Mei, C. Yu, Y. Xu, D. Han, and L. Cheng, "Effect of impact energy on damage resistance and mechanical property of C/SiC composites under low velocity impact," *Materials Science and Engineering: A*, vol. 687, pp. 141–147, 2017.

[17] B. Li and M. S. Hoo Fatt, "Hoo Fatt. Impact damage and residual strength prediction of 2D woven SiC/SiC composites," *Finite Elements in Analysis and Design*, vol. 113, pp. 30–42, 2016.

[18] Y. Yang, X. Fei, Z. Yueqing et al., "Numerical simulation on low-speed impact response of 2D plain-woven C/SiC composite," *Explosion and Shock Wave*, vol. 35, no. 1, pp. 22–28, 2015, in Chinese.

[19] H. P. Qiu, S. H. Liu, L. Wang et al., "The matrix cracking stress and residual thermal stress of 2D SiC/SiC composite fabricated by PIP process," *Solid State Phenomena*, vol. 281, pp. 375–381, 2018.

[20] ASTM D7136/D7136M – 05, *Standard Test Method for Measuring the Damage Resistance of a Fiber-Reinforced Polymer Matrix Composite to a Drop-Weight Impact Event*, ASTM International, West Conshohocken, PA, USA, 2020.

[21] J. Zhou, B. Liao, Y. Shi, Y. Zuo, H. Tuo, and L. Jia, "Low-velocity impact behavior and residual tensile strength of CFRP laminates," *Composites Part B: Engineering*, vol. 161, pp. 300–313, 2019.

[22] B. Liu, Y. Gao, Z. Tan et al., "Experimental study of low energy level impact damage on 2D C/SiC composites," *Journal of Aeronautics*, vol. 42, pp. 1–13, 2020, Chinese.